Applicability of coupling strength estimation for linear chains of restricted access*

He Feng(冯赫)[1,2], Tian-Min Yan(阎天民)[1,†], and Yuhai Jiang(江玉海)[1,2,3,‡]

[1] *Shanghai Advanced Research Institute, Chinese Academy of Sciences, Shanghai* 201210, *China*
[2] *University of Chinese Academy of Sciences, Beijing* 100049, *China*
[3] *School of Physical Science and Technology, ShanghaiTech University, Shanghai* 201210, *China*

(Received 11 September 2019; revised manuscript received 25 December 2019; accepted manuscript online 16 January 2020)

The characterization of an unknown quantum system requires the Hamiltonian identification. The full access to the system, however, is usually restricted, hindering the direct retrieval of the relevant parameters, and a reliable indirect estimation is usually required. In this work, based on the reformulated form of the original algorithm of Burgarth *et al.* [*Phys. Rev. A* **79** 020305 (2009)], the robustness of the estimation scheme against numerous sources of errors during the actual measurement is analyzed. The scheme is numerically studied for sites with a chain structure, exploring its applicability against observational errors including the limited signal-noise ratio and the finite spectral width. The spectral distribution of the end site is shown to determine the applicability of the method, and reducing the influence from truncated spectral components is critical to realize the robust reconstruction of the coupling strengths.

Keywords: Hamiltonian estimation, spin chain, state transfer

PACS: 03.65.–w, 03.65.Wj, 03.67.Ac **DOI:** 10.1088/1674-1056/ab6c43

1. Introduction

The accurate control of the Hamiltonian of the designed systems is always a prerequisite to carry out desired tasks, e.g., quantum computation,[1,2] quantum communication,[3] and quantum metrology.[4–7] The systems are usually microscopic structures which are delicately engineered to realize specific functions. To verify and benchmark these fabricated structures, the characterization of the system via Hamiltonian identification is desired.[8] Usually, the dynamics within the system are extremely complicated, and the probing access is often restricted. A delicately devised identification scheme is supposed to allow the sensible estimation of the unknown parameters, reconstructing the Hamiltonian indirectly based on partially available information, e.g., the *a priori* knowledge about the structure of the quantum network, the initial state, or an accessible subset of observables, *et al.*

Under the challenge of complicated dynamics and restricted addressing resources, various identification algorithms have been developed aiming at experimental realizations. In a many-body system, the dynamical decoupling technique, which simplifies the problem by decoupling each pair of qubits from the rest, allows for the Hamiltonian identification with arbitrary long-range couplings between qubits.[9] Besides, the dynamics can be altered by tuning the control pulse that is applied to the probe spin, improving the precision of the estimation scheme.[10,11] In a network of limited access, the identification scheme is intended to bridge the Hamiltonian parameters and the observables from accessible subsystems that are relatively easy to measure. The system realization theory is proposed for the temporal record of the observables of a local subsystem,[12,13] which has been experimentally demonstrated on a liquid nuclear magnetic resonance quantum information processor.[14] The Zeeman marker protocol shows that local field-induced spectral shifts can be used to estimate parameters in spin chains or networks.[15] Also, when the graph infection rule is satisfied, the similar parameter estimation is also available by utilizing the spectral information retrieved from a partially accessible spin.[16,17] Recently, a framework for inferring local Hamiltonians is proposed that recovers a short-ranged Hamiltonian on a large system by measuring the observables in a Gibbs state or a single eigenstate.[18]

In this work, we revisit the estimation algorithm proposed in Ref. [16] and focus on its applicability when the acquired initial data deviate from the actual values. The procedure, probing the global properties from a local site, is similar to the estimation of spring constants in classical-harmonic oscillator chains. By accessing only the end of the linear chain, the algorithm allows deducing all coupling strengths from the data of the associated spectral information. Nevertheless, the errors of the input data are inevitable and may significantly influence the reconstruction results. The simulations show that the spectral distribution is an important indicator of the applicability of the algorithm. Examining the spectral distribu-

*Project supported by Shanghai Sailing Program, China (Grant No. 16YF1412600) and the National Natural Science Foundation of China (Grant Nos. 11420101003, 11604347, 11827806, 11874368, and 91636105).

†Corresponding author. E-mail: yantm@sari.ac.cn
‡Corresponding author. E-mail: jiangyh@sari.ac.cn

tion, the increasing number of spectral components that approach zero are likely to fail the reconstruction. The applicability depends on both the properties of the individual system and conditions of measurement. Though there exist various Hamiltonian identification techniques (e.g., the ERA), the chain structure investigated here being simple allows for the direct presentation of the reconstruction procedure in our work to estimate the Hamiltonian parameter and elucidate possible sources of errors in the restricted system. Moreover, the simplicity of the original model and the explicit recursive formula allow us to track intuitively how the initial measurement errors propagate along the chain and to quantitatively assess the robustness of the reconstruction algorithm. The work is organized as follows. In Section 2, the recursive relations among spectral coefficients and coupling strengths from adjacent sites are derived. In Section 3, the robustness and the availability of the algorithm are discussed under different conditions when the input errors are introduced.

2. Theory of coupling strength estimation

We consider the state transfer within a system governed by the generic Schrödinger equation $\mathrm{i}\partial_t|\Psi(t)\rangle = \hat{H}|\Psi(t)\rangle$. With the wave function represented in basis set $\{|i\rangle\}$, $|\Psi(t)\rangle = \sum_i c_i(t)|i\rangle$, the Hamiltonian is $\hat{H} = \sum_i \varepsilon_i|i\rangle\langle i| + \sum_{i\neq j} J_{i,j}|i\rangle\langle j|$ with ε_i the on-site energy and $J_{i,j}$ the coupling strength. Thus, the Schrödinger equation in the matrix form reads

$$\dot{c}_i = -\mathrm{i}\varepsilon_i c_i - \mathrm{i}\sum_{k\sim i} J_{i,k}c_k, \tag{1}$$

where the symbol "$\sim$" means the two sites are coupled. With amplitude $c_i = \langle i|\Psi(t)\rangle$ represented spectrally, $c_i = \sum_n C_{i,n}\mathrm{e}^{-\mathrm{i}\lambda_n t}$, where $C_{i,n} = \langle i|\lambda_n\rangle\langle\lambda_n|\psi(0)\rangle$ is the spectral coefficient of mode n. The relation of $C_{i,n}$ among the coupled sites reads

$$C_{i,n} = \frac{1}{\lambda_n - \varepsilon_i}\sum_{k\sim i} J_{i,k}C_{k,n}. \tag{2}$$

The relation allows estimating the parameters using the information retrieved from a subset of sites under the restricted-access condition. The simplest example is a linear chain as shown in Fig. 1, where only the leftmost site 1 is accessible. Given an N-site chain with energies ε_i known, all coupling strengths $J_{i,i+1}$ can be reconstructed using the spectral information simply read from site 1.

The feasibility of the scheme can be shown by the repetitive use of Eq. (2) and the normalization condition $\langle i|i\rangle = 1$. Given the eigenmode n, the $C_{1,n}$ of the leftmost site 1 allows deriving $C_{2,n}$ of the next one,

$$C_{2,n} = \frac{\lambda_n - \varepsilon_1}{J_{12}}C_{1,n}. \tag{3}$$

Given that only $J_{i,k}$ with $k = i\pm 1$ are nonvanishing in the linear chain, the repetitive use of Eq. (2) yields the coefficients of subsequent sites recursively,

$$C_{i+1,n} = \frac{(\lambda_n - \varepsilon_i)C_{i,n} - J_{i-1,i}C_{i-1,n}}{J_{i,i+1}}. \tag{4}$$

The denominator $J_{i,i+1}$ should be non-zero, since a "broken" coupling forbids the retrieval of the information on the further site. Equations (3) and (4) allow for the recursive evaluation of $C_{i+1,n}$ from $C_{i,n}$ and $C_{i-1,n}$.

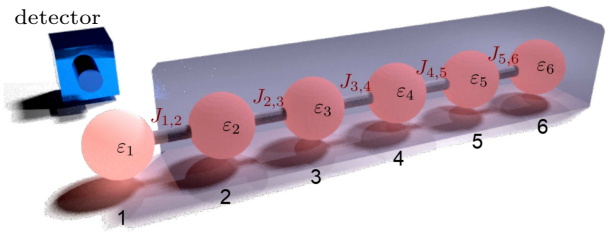

Fig. 1. Schematics of parameter estimation for a chain of N sites. Assuming that the access of the chain is restricted, only site 1, the left-most site of the chain, can be measured by the detector and all the rest (sites $2,3,\ldots,N$) are concealed by a blackbox. Using the scheme of parameter estimation, however, all coupling strengths, $J_{i,i+1}$, can be estimated if the spectral information of site 1 is available.

On the other hand, the normalization condition $\langle i|i\rangle = 1$ should be satisfied. With $C_{i,n} = \langle i|\lambda_n\rangle\langle\lambda_n|\psi(0)\rangle$, we have $\langle i|i\rangle = \sum_n\langle i|\lambda_n\rangle\langle\lambda_n|i\rangle = \sum_n|\frac{C_{i,n}}{\langle\lambda_n|\psi(0)\rangle}|^2 = 1$. The unknown denominator $\langle\lambda_n|\psi(0)\rangle$ depends on the concrete form of the initial state $|\psi(0)\rangle$. If the system is initially prepared by populating state $|1\rangle$ only, as considered in our case, $|\psi(0)\rangle = |1\rangle$, the denominator reads $|\langle\lambda_n|\psi(0)\rangle|^2 = |\langle\lambda_n|1\rangle|^2 = C_{1,n}$ and the normalization condition becomes

$$\langle i|i\rangle = \sum_n \frac{|C_{i,n}|^2}{C_{1,n}} = 1. \tag{5}$$

With only state $|1\rangle$ accessible, the information of $|1\rangle$, $c_1(t) = \sum_n C_{1,n}\mathrm{e}^{-\mathrm{i}\lambda_n t}$, is supposed to be acquired by the measurement, providing the input values of $C_{1,n}$ and λ_n for further parameter estimation. The measured $C_{1,n}$ should be normalized by Eq. (5). Next, substituting Eq. (3) into Eq. (5) with $i = 2$, the normalization condition $\langle 2|2\rangle = 1$ yields

$$J_{1,2} = \sqrt{\sum_n^N |\lambda_n - \varepsilon_1|^2 C_{1,n}} \tag{6}$$

and the normalized $C_{2,n}$ using Eq. (3). With the evaluated $J_{i-1,i}$, $C_{i,n}$, and $C_{i-1,n}$, equation (5) generates $J_{i,i+1}$ for $i \geqslant 2$,

$$J_{i,i+1} = \sqrt{\sum_n^N \frac{|(\lambda_n - \varepsilon_i)C_{i,n} - J_{i-1,i}C_{i-1,n}|^2}{C_{1,n}}}. \tag{7}$$

Hence, all coupling strengths can be recursively evaluated based on the above derived Eqs. (3), (4), (6), and (7).

In a realistic experimental setup, the above scheme works for any system that can be reduced to the form equivalent to Eq. (1). In Ref. [17], the method is applied to the N-spin chain described by Heisenberg Hamiltonian

$$\hat{H} = \sum_i^{N-1} J_{i,i+1}(\sigma_i^+\sigma_{i+1}^- + \sigma_i^-\sigma_{i+1}^+ + \Delta\sigma_i^z\sigma_{i+1}^z), \tag{8}$$

with Δ the anisotropy, $J_{i,i+1}$ the nearest-neighbor interaction strength, and $\sigma^{\pm}$ the spin raising and lowering operators, $\sigma^{\pm} = \frac{\sigma^x \pm \mathrm{i}\sigma^y}{2}$. $\hat{H}$ acts on the 2^N-dimensional Hilbert space of the N-spin chain $\mathscr{H} = \bigotimes_{i=1}^{N} \mathscr{H}_i = (\mathbb{C}^2)^{\otimes N}$, where $\mathscr{H}_i$ is a two-dimensional vector space over $\mathbb{C}$ spanned by the standard basis $|0\rangle$ and $|1\rangle$ corresponding to states of spin-up $|\uparrow\rangle$ and spin-down $|\downarrow\rangle$, respectively. The total z-component of the spins, $\sigma^z_{\text{total}} = \sum_i \sigma^z_i$, is conversed, i.e., $[\sigma^z_{\text{total}}, \hat{H}] = 0$, which means $\mathscr{H}$ can be decomposed into $N+1$ subspaces $\mathscr{H}^{(n)}$ according to the number of excitations (spin-ups) $n = 0, 1, \ldots, N$, $\mathscr{H} = \bigoplus_{n=0}^{N} \mathscr{H}^{(n)}$. For the purpose to estimate the unknown parameters as in Ref. [16], we restrict $\mathscr{H}$ to the single excitation subspace $\mathscr{H}^{(1)}$ spanned by the basis vectors $\{|i\rangle, i = 0, 1, \ldots, N\}$, where i indicates the position of the excitation. Hence, we can alternatively map the spin chain containing a single excitation to a multi-state single particle system of chain-like structure. Assuming the system is prepared within the single excitation section, the subsequent evolution under the Hamiltonian (8) is still restricted to the single excitation sector. The time evolution is mapped to the generic Schrödinger equation for a single particle, Eq. (1), where the energies are given by $\varepsilon_i = \Delta \left[\sum_{j=1}^{N-1} J_{j,j+1} - 2(J_{i,i+1} + J_{i-1,i})\right]$. Since the influence from disorder is not of concern in this work, all energies ε_i are zero, i.e., $\Delta = 0$, as will also be considered in the following discussion. The values of $C_{1,n}$ are embedded in the reduced density matrix of $|1\rangle$, which can be experimentally obtained by quantum state tomography.[17] Here, we are not concerned with the specific realization of the measurement, Hence, the input variables λ_n and $C_{1,n}$ are assumed to be readily reachable, but they are not necessarily guaranteed to be completely precise, as will be discussed later.

The initial state of the entire spin chain system for the probing in the reconstruction algorithm can be chosen as $|\Psi(0)\rangle = \alpha|0_1 00\ldots0\rangle + c|1_1 00\ldots0\rangle = \alpha|\mathbf{0}\rangle + c|\mathbf{1}\rangle$, which means that only the leftmost spin has been excited to the $|1\rangle$ state. For our purpose of unknown parameters estimation, it suffices to restrict $\hat{H}$ to the single excitation subspace $\mathscr{H}^{(1)}$. As the ground state $|\mathbf{0}\rangle$ is the eigenstate of $\hat{H}$, α dose not change during the evolution. Thus, at time t, the initial state $|\Psi(0)\rangle$ evolves to $|\Psi(t)\rangle = \alpha|\mathbf{0}\rangle + \sum_{i=1}^{N} c_i(t)|i\rangle$ with complex coefficients α and $c_i(t)$, where $|\alpha|^2 + \sum_{i=1}^{N} |c_i(t)|^2 = 1$. The initial conditions are then given by $c_1(0) = c$ and $c_i(0) = 0$ (for all $i \neq 1$). The spin chain system can be initialized in $\alpha|\mathbf{0}\rangle + c|\mathbf{1}\rangle$ by acting on the leftmost spin 1 only.[16] Then, by performing quantum-state tomography on spin 1 after time t, we can measure the element of the reduced density matrix of spin 1, $\langle\mathbf{1}|\mathrm{e}^{-\mathrm{i}\hat{H}t}|\mathbf{1}\rangle = \sum_n \mathrm{e}^{-\mathrm{i}\lambda_n t}|\langle\mathbf{1}|\lambda_n\rangle|^2$. And the eigenvalues $\{\lambda_n\}$ and the spectral coefficients $\{C_{1,n} = |\langle\mathbf{1}|\lambda_n\rangle|^2\}$ can be obtained through Fourier transform, which are the input variables of the reconstruction algorithm.

As a simple example, the estimation of $J_{i,i+1}$ in a chain with 6 sites is demonstrated in Fig. 2. With only site 1 accessible, the time evolution of state $|1\rangle$ [Fig. 2(a)] is supposed to be detectable. In the associated spectral distribution [Fig. 2(b)], the position and the height of each spectral peak provide λ_n and $C_{1,n}$, respectively, as required input values for the estimation scheme. Performing the evaluation using Eqs. (3), (4), (6), and (7) recursively, we successfully reconstruct all the five unknown coupling strengths $J_{i,i+1}$, as shown in Fig. 2(c).

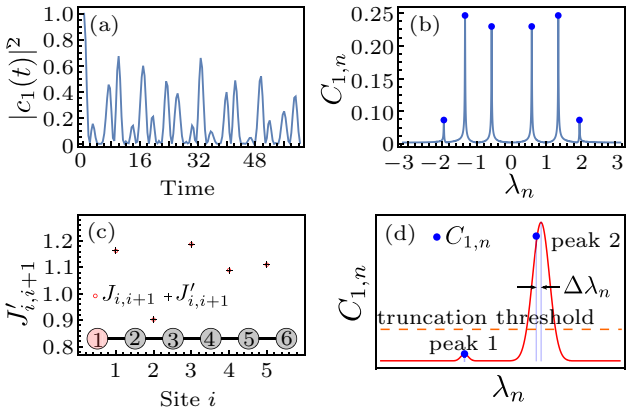

Fig. 2. Reconstruction of $J_{i,i+1}$ for a chain of $N = 6$ and $\varepsilon_i = 0$. Panel (a) shows the temporal evolution of population on site 1, and panel (b) shows its spectral distribution that provides λ_n and $C_{1,n}$ as required by the reconstruction algorithm. In panel (c), applying the parameter estimation, the five unknown coupling strengths are estimated. The estimated values $J'_{i,i+1}$ show good agreement with the actual values $J_{i,i+1}$. Panel (d) presents the possible errors with the input values λ_n and $C_{1,n}$ that may hamper the reconstruction procedure. For peak 1, the $C_{1,n}$ below the threshold during the measurement is simply truncated. For peak 2, the broadening of the spectral peak results in the deviation of the measured eigenvalue λ'_n from the actual λ_n.

3. Influence from errors of input variables

During the actual measurement, the finite instrumental resolution, the limited signal-noise ratio, and other perturbations may hinder the precise acquisition of initial input λ_n and $C_{1,n}$. Therefore, the robustness of the algorithm against the deviations of these input values is critical to the success of the parameter estimation. The influence from imprecision of measured $C_{1,n}$ has been mentioned in Ref. [16], showing rather robust performance against small deviations. When the finite signal-noise ratio of the $C_{1,n}$ detection is considered, the even worse situation occurs when partial information is lost due to the truncation of small values. As shown in Fig. 2(d), the finite signal-noise ratio sets the truncation threshold. When the value of $C_{1,n}$ for peak 1 is below the line representing the threshold, the corresponding $C_{1,n}$ is missing. Besides the errors in $C_{1,n}$ which are encoded in the heights of the spectral peaks, the λ_n that are read from the positions of the peaks are also susceptible to errors during the measurement. As shown by peak 2 in Fig. 2(d), the nonvanishing spectral width caused by either the finite instrumental resolution or the fluctuation during the measurement may contribute to the uncertainty $\Delta\lambda_n$. The imprecise λ_n also deteriorates the performance of $J_{i,i+1}$-reconstruction.

We take the example of the simplest parametric setup, a chain of 100 sites with identical coupling strengths $J_{i,i+1}=1$ and energies $\varepsilon_i=0$, to show how the input values influence the results. Under the ideal condition without any deviations of λ_n and $C_{1,n}$, the simulated results show that $J_{i,i+1}$ can be correctly recovered for a long chain (tested up to thousands sites). In a realistic experiment, however, the spectral peaks of small-valued $C_{1,n}$ may not be well resolved, or even simply be truncated. With the less number of observed peaks than the actual one, the lost information does influence the reconstructed results.

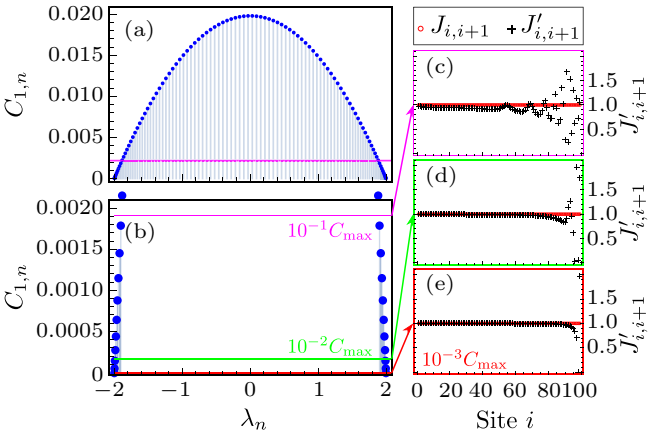

Fig. 3. For a homogeneous linear chain of $N=100$, panel (a) shows the spectral distribution $C_{1,n}$ versus λ_n. The region below $10^{-1}C_{\max}$, as indicated by the purple line in (a), is zoomed as shown in panel (b). Assuming the $C_{1,n}$ can be resolved up to 10^{-1} (purple), 10^{-2} (green), and 10^{-3} (red) of $C_{\max}$, all the input data $(\lambda_n, C_{1,n})$ with $C_{1,n}$ below the threshold are truncated. The corresponding estimated coupling strengths $J'_{i,i+1}$ are shown in (c), (d), and (e), respectively, comparing with the original coupling strengths $J_{i,i+1}$.

The influence from the truncation is shown in Fig. 3. For a homogeneous linear chain with all $\varepsilon_i=\varepsilon$ and $J_{i,i+1}=J$, the eigenvalues are given by $\lambda_n=\varepsilon+2J\cos[\pi n/(N+1)]$ for $n=1,\ldots,N$. The element of the associated eigenvector for the i-th site reads $C_{i,n}=\sin[n\pi i/(N+1)]$. For the accessible site 1, $C_{1,n}=\sin[n\pi/(N+1)]$, as shown by the spectral distribution in Fig. 3(a). The $C_{1,n}$ of small values are around both the far ends along the λ_n-axis, where the data below a given threshold are truncated if a finite signal-noise ratio is specified. For different truncation thresholds as indicated in Fig. 3(b), the estimated results of $J_{i,i+1}$ are compared in Figs. 3(c)–3(e).

Assuming that the maximum value of $C_{1,n}$ is $C_{\max}$, when the threshold is $10^{-1}C_{\max}$ with ten pairs of $C_{1,n}$ truncated, significant deviation appears from $i=50$. When the data below $10^{-2}C_{\max}$ are truncated with three pairs of $C_{1,n}$ missing, the $J_{i,i+1}$ can be correctly reconstructed up to $i=80$. Further, when only one pair of data are truncated below the threshold $10^{-3}C_{\max}$, the deviations only appear at the rightmost sites of the chain. The results suggest that the complete data of $C_{1,n}$ should be important to the success of the algorithm. More intriguingly, though all $C_{1,n}$ contribute to the evaluation of each $J_{i,i+1}$, when some components are missing, the chain can still be recovered to some extent instead of failing in the reconstruction as a whole, which shows the robustness of the algorithm.

The error $\delta J_{i,i+1}$ induced by the truncation appears to accumulate along the chain. To clarify this, we assume that a pair of small-valued input data $C_{1,m_1}=C_{1,m_2}=\delta$ for eigenvalues $\lambda_{m_1}=-\lambda_{m_2}$ are truncated during the measurement and perform perturbation analysis of error propagation with respect to δ. From Eq. (4), it shows that all $C_{i,m}$ are absent during the reconstruction as long as $C_{1,m}=\delta$ of mode m is ignored from the input data. Taking variables up to the first order of δ, the linear approximations assume $C_{i,n}=C'_{i,n}+\varsigma_{i,n}\delta(n\neq m)$, $C_{i,m}=\xi_{i,m}\delta$, and $J_{i,i+1}=J'_{i,i+1}+\theta_i\delta$, where $C'_{i,n}$ and $J'_{i,i+1}$ are the reconstructed variables tainted by the truncation, and $C_{i,n}$ and $J_{i,i+1}$ are the true values. Perturbation parameter θ_i determines the deviation of the reconstructed coupling strength $J'_{i,i+1}$ from the true value $J_{i,i+1}$. Next, we need to find $\varsigma_{i,n}$, $\xi_{i,m}$, and θ_i from the recursive relations (4) and (7). Substituting the approximations into Eq. (7) and separating the contribution of the truncated components from the rest, the recursive relation of $J_{i,i+1}$ takes the form

$$J_{i,i+1} = \sqrt{\Theta_{\text{measured}}+\Theta_{\text{truncated}}}.$$

The contributions from the acquired modes Θ_{measured} and the truncated data $\Theta_{\text{truncated}}$ are

$$\Theta_{\text{measured}} = \sum_{n\neq m_1,m_2}^{N} \frac{[\Delta_{n,i}(C'_{i,n}+\varsigma_{i,n}\delta)-(J'_{i-1,i}+\theta_{i-1}\delta)(C'_{i-1,n}+\varsigma_{i-1,n}\delta)]^2}{C_{1,n}},$$

$$\Theta_{\text{truncated}} = \sum_{m\in\{m_1,m_2\}} \frac{[\Delta_{m,i}\xi_{i,m}\delta-(J'_{i-1,i}+\theta_{i-1}\delta)\xi_{i-1,m}\delta]^2}{\delta},$$

respectively, where $\Delta_{n,i}=\lambda_n-\varepsilon_i$. Keeping terms up to the first order of δ, eventually θ_i can be determined recursively from θ_{i-1}, $\varsigma_{i-1,n}$, $\varsigma_{i,n}$, $\xi_{i-1,m}$, and $\xi_{i,m}$,

$$\theta_i = \frac{\sum_{n\neq m_1,m_2}^{N} \frac{2(\Delta_{n,i}C'_{i,n}-J'_{i-1,i}C'_{i-1,n})(\Delta_{n,i}\varsigma_{i,n}-\theta_{i-1}C'_{i-1,n}-J'_{i-1,i}\varsigma_{i-1,n})}{C_{1,n}} + \sum_{m\in\{m_1,m_2\}} (\Delta_{m,i}\xi_{i,m}-J'_{i-1,i}\xi_{i-1,m})^2}{2J'_{i,i+1}}, \quad (9)$$

with the initial condition $\theta_1 = [(\Delta_{m_1,1})^2 + (\Delta_{m_2,1})^2]/2J'_{1,2}$ according to Eq. (6).

Similarly, substituting the linear approximations into recursive relation (4), we can find the recursive formulas for $\varsigma_{i,n}$ and $\xi_{i,m}$,

$$\varsigma_{i+1,n} = \frac{\Delta_{n,i}(J'_{i,i+1}\varsigma_{i,n} - C'_{i,n}\theta_i)}{(J'_{i,i+1})^2} - \frac{J'_{i-1,i}J'_{i,i+1}\varsigma_{i-1,n} + C'_{i-1,n}J'_{i,i+1}\theta_{i-1} - C'_{i-1,n}J'_{i-1,i}\theta_i}{(J'_{i,i+1})^2}, \quad (10)$$

$$\xi_{i+1,n} = \frac{\Delta_{m,i}\xi_{i,m} - J'_{i-1,i}\xi_{i-1,m}}{J'_{i,i+1}}. \quad (11)$$

The initial conditions are $\varsigma_{1,n}=0$, $\varsigma_{2,n}=-\Delta_{n,1}\Delta^2_{m,1}C_{1,n}/2(J'_{1,2})^3$, $\xi_{1,m} = 1$, and $\xi_{2,m} = \Delta_{m,1}/J'_{1,2}$.

In Fig. 4, we present the comparisons between error estimation under the linear approximation of Eqs. (9), (10), and (11) with the results from the reconstruction algorithm under different circumstances. Figures 4(a) and 4(b) show the results for a homogeneous chain of identical coupling strengths $J_{i,i+1} = 1$ when $N = 50$ and 100, respectively. Figures 4(c) and 4(d) present the results for a non-homogeneous chain of randomly distributed $J \in [0.9, 1.1]$ when $N = 50$ and 100, respectively. In all four cases, when the error propagates along the chain, the deviations appear earlier under the linear approximation than the original algorithm. It suggests that some nonlinearity associated to the algorithm could protect the reconstruction from deterioration. In this case, the linear approximation based on the perturbation analysis may provide the lower bound of the error introduced by the truncation of the input data during the measurement. However, the role of nonlinearity still requires further investigation.

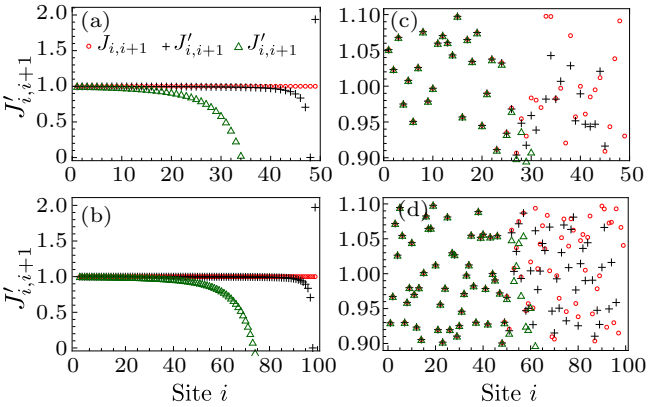

Fig. 4. Comparison among true values of $J_{i,i+1}$ (circle symbol), reconstructed $J'_{i,i+1}$ (cross symbol), and predicted $J'_{i,i+1}$ (triangle symbol) from perturbation analysis under the linear approximation when (a) $N = 50$ and $J_{i,i+1} = 1$, (b) $N = 100$ and $J_{i,i+1} = 1$, (c) $N = 50$ and random $J_{i,i+1} \in [0.9, 1.1]$, and (d) $N = 100$ and random $J_{i,i+1} \in [0.9, 1.1]$. The reconstruction starts with a pair of $C_{1,n}$ truncated.

Next, we consider the estimation when $J_{i,i+1}$ vary with i, as we desired in practice. Without loss of generality, the $J_{i,i+1}$ are randomly chosen within a given interval, i.e., the disorder induced by $J_{i,i+1}$. It is shown that the interval is highly relevant to the performance of the estimation. Figures 5(a) and 5(b) present the dependence of the reconstruction on the interval. In Fig. 5(a), when the span is small, $J_{i,i+1} \in [0.9, 1.1]$, the $J_{i,i+1}$ can be correctly estimated up to $i = 28$. While when the span is large, $J_{i,i+1} \in [0.8, 1.2]$, the applicability deteriorates, the estimated values $J'_{i,i+1}$ start deviating from $J_{i,i+1}$ around site 16, as can be straightforwardly read from the error defined by $\delta J_{i,i+1} = J'_{i,i+1} - J_{i,i+1}$ as shown in Fig. 5(c).

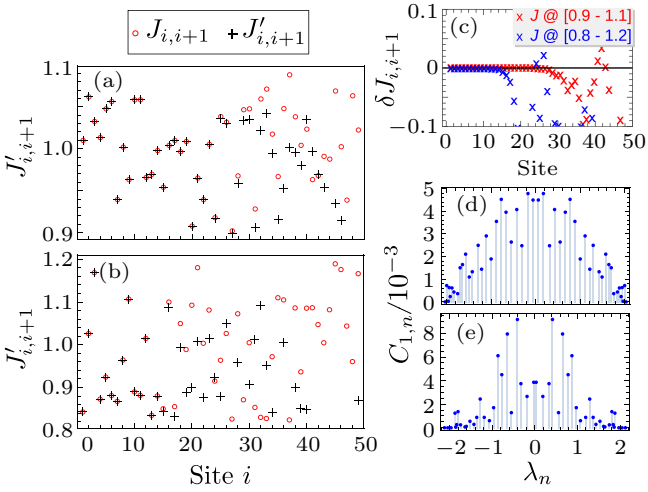

Fig. 5. Estimation of $J_{i,i+1}$ in a chain of $N = 50$ when $C_{1,n}$ is resolved up to 10^{-3}. The $J_{i,i+1}$ are randomly distributed in range (a) $[0.9, 1.1]$ and (b) $[0.8, 1.2]$. The errors $\delta J_{i,i+1} = J'_{i,i+1} - J_{i,i+1}$ for the two different intervals are compared in panel (c). Panels (d) and (e) show distributions of input data $C_{1,n} = |\langle\lambda_n|1\rangle|^2$ on site 1 for $J_{i,i+1} \in [0.9, 1.1]$ and $J_{i,i+1} \in [0.8, 1.2]$, respectively, to reconstruct $J_{i,i+1}$ as shown in (a) and (b).

As discussed above, the reconstruction is rather robust for a long chain with identical $J_{i,i+1}$. When $J_{i,i+1}$ are randomly distributed, however, the effective distance of reconstruction is significantly shortened, showing an anticorrelation between the distance and the distribution interval of $J_{i,i+1}$. Examining the spectral distribution, the anticorrelation can also be explained by the truncation of $C_{1,n}$ as discussed for the homogeneous chain. The distribution interval of $J_{i,i+1}$ influences the spectral pattern and the probability to find $C_{1,n}$ around zero. With the distribution of random $J_{i,i+1}$ broadened, the spectral distribution in Figs. 5(d) and 5(e) is no more as regular as that in the homogeneous chain. The $C_{1,n}$ scatter to a larger range with the increasing distribution interval of $J_{i,i+1}$, and more $C_{1,n}$ approach zero. As discussed for the homogeneous chain, these near-zero $C_{1,n}$ are likely to be truncated, and the resultant lost spectral components worsen the applicability of the algorithm. In addition, it is found that the decreasing $J_{i,i+1}$ also lowers the value of $C_{1,n}$ and impedes the parameter estimation, as can be intuitively understood since any broken bridge hinders the probe of further sites. The above discussion also applies when disorders of ε_i are involved as the spectral distribution also presents the similar pattern and suggests the involvement of the localization.

Besides the influence from the errors of $C_{1,n}$, the measurement of λ_n also affects the $J_{i,i+1}$ reconstruction. Assuming the actual eigenvalue is λ_n, the restricted resolution or disturbance during the experiment may deviate the measured value from λ_n, $\lambda_n' = \lambda_n + \Delta\lambda_n$. The fluctuation $\Delta\lambda_n$ in each measurement results in the difference of the estimated $J'_{i,i+1}$, as illustrated in Fig. 2(d). The eventual $J'_{i,i+1}$ should be the average of the reconstructed results after multiple measurements. We examine the parameter reconstruction when fluctuations $\Delta\lambda_n$ around the true value of λ_n are involved. An example for a chain of $N = 100$ with coupling strengths $J_{i,i+1} \in [0.9, 1, 1]$ is shown in Fig. 6(a), where all coupling strengths can be precisely reconstructed if no random error is introduced. To account for the influence from nonvanishing random errors, each of $\Delta\lambda_n$ is chosen randomly for a single measurement, and the samples are generated from a normal distribution, $\Delta\lambda_n \sim \mathcal{N}(0, \sigma^2)$. Then we perform multiple simulated measurements and evaluate the averaged $J'_{i,i+1}$. Figure 6(b) shows the averaged $J'_{i,i+1}$ from 2000 simulated measurements when $\sigma = 0.001$. Here, the influence of the truncation of small-valued $C_{1,n}$ is neglected.

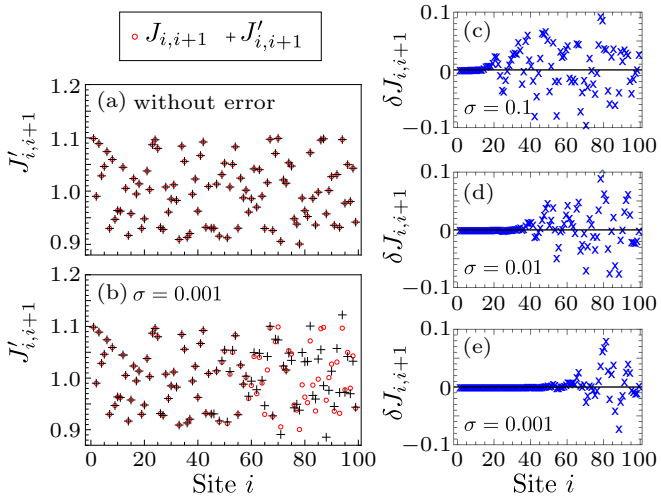

Fig. 6. The estimation of coupling strengths when $\Delta\lambda_n$ is considered for each measurement. In a chain of 100 sites with $J_{i,i+1} \in [0.9, 1.1]$, the reconstructed $J'_{i,i+1}$ are compared with $J_{i,i+1}$ in (a) when $\Delta\lambda_n = 0$. In (b), the reconstructed $J'_{i,i+1}$ are shown when $\sigma = 0.001$. The errors $\delta J_{i,i+1}$ are presented in (c), (d), and (e) for $\sigma = 10^{-1}$, 10^{-2}, and 10^{-3}, respectively.

From errors $\delta J_{i,i+1}$ as shown in Figs. 6(c)–6(e), the $J_{i,i+1}$ can be roughly estimated up to $i = 20$, 40, and 60, respectively, for $\sigma = 10^{-1}$, 10^{-2}, and 10^{-3}. While without $\Delta\lambda_n$ fluctuation [Fig. 6(a)], all $J_{i,i+1}$ are correctly reconstructed. For the chain of $N = 100$, the average and minimum gaps of λ_n are 0.04 and 0.002, respectively. The average gap is larger than the fluctuations considered in Figs. 6(e) ($\sigma = 0.001$) and 6(d) ($\sigma = 0.01$) so that the spectral peaks are supposed to be resolved. For comparison, figure 6(c) takes $\sigma = 0.1$ which is large, showing the expected failure of the reconstruction scheme when the spectral peaks cannot be well resolved. Therefore, the precise measurement λ_n is shown to be critical to the precise reconstruction. For a longer chain, we do not find significant deviations. However, the denser spectral distribution with more states involved will hinder the precise retrieval of λ_n, if the instrumental resolution of λ_n-acquisition is finite.

4. Conclusion

The reconstruction of parameters within a partially accessible system is an important problem when indirect probing is the only option to acquire the desired information. In this work, the algorithm to estimate parameters in a linear chain with restricted access is extensively investigated, providing the necessary information to assess the algorithm robustness. Starting with the generic Schrödinger equation, it is confirmed that the coupling strengths can be efficiently deduced from the recursive relation using the spectral information of only the end site. We focus on the applicability of the algorithm, which is shown to be highly relevant to the spectral distribution on the accessible site. Given the errors induced by the finite signal-noise ratio, the increasing number of truncated spectral components is shown to gradually deteriorate the reconstruction performance. It is found that reducing the loss of spectral components is critical to the success of the method. Even so, the partially successful estimation in the presence of truncations shows the robustness of the algorithm and the estimation can be conducted in a controllable way. Since the spectral distribution is system dependent, the applicability of the method also varies with the systems. Accordingly, it is advisable to understand the nature of the system before applying the method.

References

[1] Ladd T D, Jelezko F, Laflamme R, Nakamura Y, Monroe C and O'Brien J L 2010 *Nature* **464** 45
[2] Bassett L C and Awschalom D D 2012 *Nature* **489** 505
[3] Bose S 2003 *Phys. Rev. Lett.* **91** 207901
[4] Giovannetti V, Lloyd S and Lorenzo Maccone 2006 *Phys. Rev. Lett.* **96** 010401
[5] Giovannetti V, Lloyd S and Lorenzo Maccone 2011 *Nat. Photon.* **5** 222
[6] Xiang G Y and Guo G C 2013 *Chin. Phys. B* **22** 110601
[7] Zhang L J and Xiao M 2013 *Chin. Phys. B* **22** 110310
[8] Cole J H 2015 *New J. Phys.* **17** 101001
[9] Wang S T, Deng D L and Duan L M 2015 *New J. Phys.* **17** 93017
[10] Kiukas J, Yuasa K and Burgarth D 2017 *Phys. Rev. A* **95** 052132
[11] Liu J and Yuan H D 2017 *Phys. Rev. A* **96** 012117
[12] Zhang J and Sarovar M 2014 *Phys. Rev. Lett.* **113** 080401
[13] Zhang J and Sarovar M 2015 *Phys. Rev. A* **91** 052121
[14] Hou S Y, Li H and Long G L 2017 *Sci. Bull.* **62** 863
[15] Burgarth D and Ajoy A 2017 *Phys. Rev. Lett.* **119** 030402
[16] Burgarth D, Maruyama K and Nori F 2009 *Phys. Rev. A* **79** 020305
[17] Burgarth D and Maruyama K 2009 *New J. Phys.* **11** 103019
[18] Bairey E, Arad I and Linder N H 2019 *Phys. Rev. Lett.* **122** 020504